Resolution Analysis of Bistatic SAR

Guillermo Garza and Zhijun Qiao

Department of Mathematics, The University of Texas-Pan American
1201 W. University Drive, Edinburg,TX USA 78539

ABSTRACT

In this paper, we analyze the resolution of bistatic synthetic aperture radar (BISAR) imaging for stationary objects. In particular, we analyze the resolution of images reconstructed by the method of a filtered backprojection inversion, an inversion method which is derived from a scalar wave equation model. In this context we are able to account for the effects of antenna beam patterns and arbitrary flight trajectories. The analysis is done by examining the data collection manifold for different experiment geometries and system parameters.

Keywords: SAR, Imaging, BISAR, image formation, backprojection

1. INTRODUCTION

In synthetic aperture radar (SAR) imaging, radar antennas are mounted on an airborne platform. The scene to be imaged is illuminated by electromagnetic waves transmitted from an antenna. The goal is to reconstruct an image of the scene from the measurements taken of the scattered waves. In general, the resolution of the image is better for larger bandwidths and longer flight trajectories. In addition, the resolution is affected by the beam patterns of both the antenna transmitting the waves and the antenna measuring the scattered waves. For a given experiment we refer to the flight trajectory, transmit and receive beam patterns as the experiment geometry, and we refer to the carrier frequency and bandwidth as the system parameters. In this paper, we explicitly relate the experiment geometry and system parameters to image resolution in the context of the model and inversion method described in Ref. 1–3. Though in some respects the limits of SAR image resolution are well known,[4,5] we believe this treatment best relates image resolution to experiment geometry and system parameters together. Our analysis is similar to the idea of Fourier space coverage of the Fourier diffraction theorem,[6] but also incorporates antenna beam patterns.

We study images formed by a filtered backprojection inversion. The backprojection operator used is an approximate inverse operator for the system model, with a few caveats when applied. First, the system model and the equation for the measured data are derived from a scalar wave-equation model, which is itself derived from Maxwell's equations for electromagnetism. However, the model does not incorporate all predicted behavior of electromagnetic waves. In particular, since it is a scalar model it does not describe the vector nature of electromagnetic waves and therefore doesn't incorporate the effects of polarization. Even so, the equation for the measured data is consistent with the most commonly used models for SAR imaging. Second, the model makes a single scattering assumption, known as the Born-approximation, which has the effect of linearizing the model. This linearization is what makes an inversion possible. Again the use of the Born-approximation is consistent with most SAR imaging models. Also, in order to perform the inversion we must make the assumption that the only sources of electromagnetic radiation are from the transmitter. In practice, the ubiquitous presence of noise in the measured data will always make an exact inversion impossible. However, statistical methods applied to the same model can be used to form images that suppress the effects of noise and also clutter.[7] Finally, we make the assumption that the target reflects equally from all perspectives.

This paper is organized as follows. In Section 2 we introduce the model under which we perform our analysis. In Section 3 we present the point spread function, which is the main subject of our analysis. Finally, in Section 4 we examine the resolution achieved for different experiment geometries and system parameters.

Further author information: (Send correspondence to Z.Q.)
G.G.: E-mail: ggarzaz39@broncs.utpa.edu, Telephone: 1 956 292 7326
Z.Q.: E-mail: qiao@utpa.edu, Telephone: 1 956 381 3406

Radar Sensor Technology XV, edited by Kenneth I. Ranney, Armin W. Doerry,
Proc. of SPIE Vol. 8021, 80211V · © 2010 SPIE · CCC code: 0277-786X/10/$18 ·
doi: 10.1117/12.884068

2. MODEL

For our purposes we consider Monostatic SAR to be a special case of Bistatic SAR. We call the antenna illuminating the scene the transmitting antenna, and we call the antenna recording measurements the receiving antenna. We begin by describing the forward model. Following Ref. 1–3, this model is derived from a scalar wave model where the location of scatterers causes disruptions in the speed of propagating waves. The reflectivity function is

$$V(\boldsymbol{x}) = \frac{1}{c_0^2} - \frac{1}{c(\boldsymbol{x})^2}$$

where $c(\boldsymbol{x})$ is the wave speed at position $\boldsymbol{x}$ and c_0 denotes the speed of light in a vacuum. The location of scatterers in the target scene correspond to the location of singularities in V. The goal is to reconstruct V from the measurements of the scattered waves.

The time-varying data d measured by the receiving antenna at a position parameterized by s is modeled as

$$d(s,t) = \mathcal{F}\{V\}(s,t) = \int\int \mathrm{e}^{-2\pi i f(t-R(s,\boldsymbol{x})/c_0)} A(s,\boldsymbol{x},f) V(\boldsymbol{x})\,\mathrm{d}f\,\mathrm{d}\boldsymbol{x} \tag{1}$$

where

$$A(s,\boldsymbol{x},f) = \frac{P(f) J_T(s,\boldsymbol{x},f) J_R(s,\boldsymbol{x},f)}{4\pi|\Gamma_T(s)-\boldsymbol{x}|\,|\Gamma_R(s)-\boldsymbol{x}|}, \tag{2}$$

$\Gamma_T(s)$, $\Gamma_R(s)$ denote the positions of the transmitting and receiving antenna respectively, $P(f)$ denotes the Fourier transform of the transmitted signal, and $J_T(s,\boldsymbol{x},f)$, $J_R(s,\boldsymbol{x},f)$ denote the transmitting and receiving antenna beam patterns respectively. Also, $R(s,\boldsymbol{x}) = |\Gamma_T(s)-\boldsymbol{x}| + |\Gamma_R(s)-\boldsymbol{x}|$. We assume the transmitting antenna transmits band-limited signals.

With the additional assumption that the antennas are broadband and an appropriate symbol estimate of A, $\mathcal{F}$ is a Fourier integral operator.[8,9] With this assumption, we can construct an approximate inverse operator, which we denote $\mathcal{B}$.

The reconstucted image $\tilde{V}$ is formed by applying the inverse operator $\mathcal{B}$ to the data d where $\mathcal{B}$ is of the form

$$\tilde{V}(\boldsymbol{z}) = \mathcal{B}\{d\}(\boldsymbol{z}) = \int\int \mathrm{e}^{2\pi i f(t-R(s,\boldsymbol{x})/c_0} Q(s,\boldsymbol{z},f) d(s,t)\,\mathrm{d}f\,\mathrm{d}s\,\mathrm{d}t. \tag{3}$$

With an appropriate choice for Q, it has been shown that singularities in the reflectivity function V appear correctly in the reconstructed image.[10] In this paper, we only evaluate the backprojection operator with a choice for Q that seeks to invert the forward operator. However, one can choose Q to suppress the effects of noise and undesirable targets, known as clutter.[7]

3. POINT SPREAD FUNCTION

We can rewrite (3) using (1) as

$$\tilde{V}(\boldsymbol{z}) = \int L(\boldsymbol{z},\boldsymbol{x}) V(\boldsymbol{x})\,\mathrm{d}\boldsymbol{x}. \tag{4}$$

where

$$L(\boldsymbol{z},\boldsymbol{x}) = \int \mathrm{e}^{2\pi i f(R(s,\boldsymbol{x})+R(s,\boldsymbol{z}))/c_0} A(s,\boldsymbol{x},f) Q(s,\boldsymbol{z},f)\,\mathrm{d}f\,\mathrm{d}s \tag{5}$$

Two point scatterers at positions $\boldsymbol{x_0}, \boldsymbol{x_1}$ are represented by the reflectivity function

$$V(\boldsymbol{x}) = \delta(\boldsymbol{x}-\boldsymbol{x_0}) + \delta(\boldsymbol{x}-\boldsymbol{x_1}).$$

Substituting into (3), we find that the resulting image is

$$\tilde{V}(\boldsymbol{z}) = L(\boldsymbol{z},\boldsymbol{x_0}) + L(\boldsymbol{z},\boldsymbol{x_1}).$$

These scatterers will be resolved independently if the support of $L(\boldsymbol{z}, \boldsymbol{x_0})$ and $L(\boldsymbol{z}, \boldsymbol{x_1})$ do not overlap. The more localized the support of $L(\boldsymbol{z}, \boldsymbol{x})$, the more accurately it represents point scatters in the scene and the better we will be able to identify fine details in the target scene. It defines the fidelity with which the scheme will produce an image of the target scene. Thus, we call $L(\boldsymbol{z}, \boldsymbol{x})$ the point spread function (PSF) of the imaging scheme. If

$$L(\boldsymbol{z}, \boldsymbol{x}) = \delta(\boldsymbol{z} - \boldsymbol{x}) = \int_{\mathbb{R}^2} \mathrm{e}^{2\pi i(\boldsymbol{z}-\boldsymbol{x})\cdot\boldsymbol{\xi}} \, \mathrm{d}\boldsymbol{\xi},$$

then the reconstructed image is exactly the reflectivity function.

Using the fundamental theorem of calculus we can write the phase of (5) as

$$\begin{aligned} 2\pi f \left(R(s, \boldsymbol{x}) + R(s, \boldsymbol{z})\right)/c_0 &= \frac{2\pi f}{c_0} \int_0^1 \frac{\mathrm{d}}{\mathrm{d}\mu} R(s, \boldsymbol{x} + \mu(\boldsymbol{z} - \boldsymbol{x})) \, \mathrm{d}\mu \\ &= 2\pi(\boldsymbol{z} - \boldsymbol{x}) \cdot \Xi(s, \boldsymbol{x}, \boldsymbol{z}, f) \end{aligned} \tag{6}$$

where

$$\boldsymbol{\Xi}(s, \boldsymbol{x}, \boldsymbol{z}, f) = \frac{f}{c_0} \int_0^1 \nabla R(s, \boldsymbol{z} + \mu(\boldsymbol{x} - \boldsymbol{z})) \, \mathrm{d}\mu \tag{7}$$

$$\approx \frac{f}{c_0} \mathcal{P}\{(\Gamma_T\widehat{(s)} - \boldsymbol{x}) + (\Gamma_R\widehat{(s)} - \boldsymbol{z})\}. \tag{8}$$

Here the operator $\mathcal{P}$ projects a vector onto its first two components. Choosing Q as in Ref. 3 and letting $\boldsymbol{\xi} = \Xi(s, \boldsymbol{x}, \boldsymbol{z}, f)$, the PSF may be rewritten as

$$L(\boldsymbol{z}, \boldsymbol{x}) = \int_\Omega \mathrm{e}^{2\pi i(\boldsymbol{z}-\boldsymbol{x})\cdot\boldsymbol{\xi}} \, \mathrm{d}\boldsymbol{\xi}. \tag{9}$$

with

$$\Omega = \{\boldsymbol{\xi} = \boldsymbol{\Xi}(s, \boldsymbol{z}, \boldsymbol{z}, f) \, : \, A(s, \boldsymbol{z}, f) \neq 0\}. \tag{10}$$

We call Ω the data collection manifold. These equations completely define the resolution of the system, which is the width of the support of $L(\boldsymbol{z}, \boldsymbol{x})$.

Note that since (1) incorporates antenna beam patterns and geometric spreading, our choice for Q necessarily includes terms that account for these. In practice most inversion schemes don't account for antenna beam patterns and some don't account for geometric spreading. In that case we may analyze the PSF written as (5) with an alternate Q that doesn't account for the neglected factors.

4. EXAMPLES

4.1 Monostatic Stripmap SAR with Linear Flight Trajectory

The simplest SAR system is that with a single antenna acting as both transmitter and receiver, and undergoing a linear flight trajectory. Near the origin we describe the resolution in terms of the support of the function $L(\boldsymbol{z}, 0)$. In this case the data collection manifold is a segment of an annulus, as shown in Figure 1. From (8) the width of the annulus is $2\beta/c_0$, where β is the bandwidth of the transmitted signal. The center of the annulus is $2f_c/c_0$ where f_c is the center frequency of the transmitted signal. For strip-map SAR we approximate the segment as a rectangle. If the flight trajectory is $\Gamma_T(s) = \Gamma_R(s) = (s + \alpha, 0, h)$, then the height of the segment is determined by the values of s for which the origin is illuminated by the antenna, that is the values of s for which $A(s, 0, f) \neq 0$. If D_y is the beam-footprint on the ground in the direction of the flightpath, then the origin is illuminated when $s \in (-D_y, D_y)$. Then as illustrated in Figure 1 we have

$$\frac{D_y}{\alpha} = \frac{h/2}{2f_c/c_0}.$$

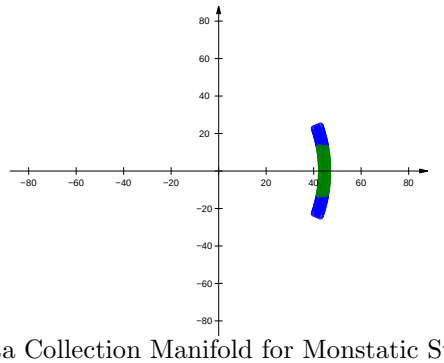

Figure 1: Data Collection Manifold for Monstatic Stripmap SAR

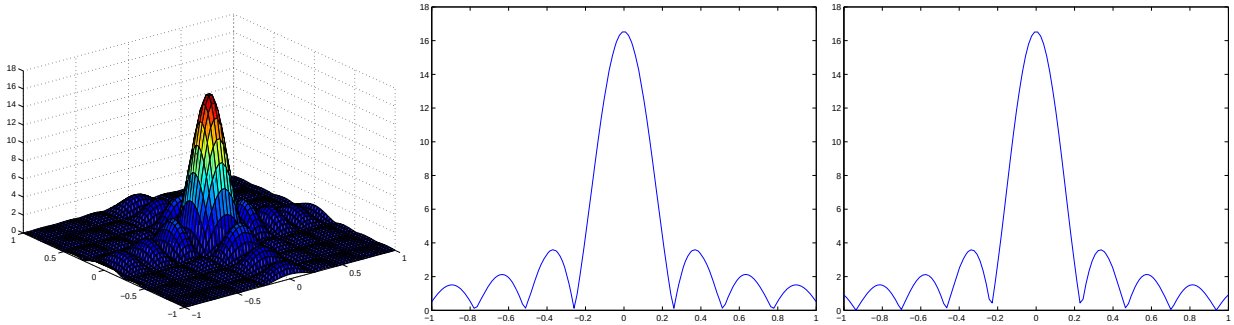

(a) 3-D view of PSF (b) Aziumth resolution (c) Range resolution

Figure 2: Point Spread Function of Monostatic Stripmap SAR

Which gives the height of the data collection manifold as $h_\Omega = \dfrac{4D_y f_c}{\alpha c_0}$.

The point spread function $L(\boldsymbol{z}, 0)$ is a 2-D Fourier transform of the shifted rectangular window

$$\chi(\boldsymbol{\xi}) = \begin{cases} 1 & \text{if } \boldsymbol{\xi} \in \Omega \\ 0 & \text{otherwise} \end{cases} \tag{11}$$

where in this case

$$\Omega = \left\{ \boldsymbol{\xi} = (\xi_1, \xi_2) : f_c - \frac{\beta}{2} < \xi_1 < f_c + \frac{\beta}{2} \ , \ |\xi_2| < |\frac{2D_y f_c}{\alpha c_0} \right\} |.$$

The width of this rectangular window is only dependent on the beamwidth, while the height is dependent on the beam-footprint. The resulting PSF is a product of sinc functions with the same property. Thus, we get the familiar result that the resolution in the direction of the flightpath, the azimuthal resolution, is dependent on the beam-footprint of the transmitting antenna, while the resolution in the direction perpendicular to the flightpath, the range resolution, is dependent only on the bandwidth of the system.

4.2 Circular Spotlight SAR

In general, imaging resolution improves for longer flight trajectories and larger bandwidths. However, since the bandwidth of any system is always finite, there is a limit to imaging resolution. This limit may be ascertained by examination of (10), the data collection manifold. We see that the all points in the data collection manifold must lie in the circle $|\boldsymbol{\xi}| < 2f_{\max}/c_0$, where $f_{\max}$ is the maximum frequency of the transmitted signal.

For monostatic SAR we see that the data collection manifold will always be segments of an annulus, with the maximum possible coverage being a full annulus of width $2\beta/c_0$. This occurs when the flight trajectory is a fill circle and the beam is fixed on the target area. This is known as Circular Spotlight SAR (CSAR). An example

of the data collection manifold for $L(\boldsymbol{z},0)$ under these conditions is shown in Figure 3. In this case we may we may think of $L(\boldsymbol{z},0)$ as a 2-D Fourier transform of a difference of cylinder functions

$$L(\boldsymbol{z},0) = \mathcal{F}\{C_1 - C_2\}(\boldsymbol{z}) \tag{12}$$

$$C_1(\boldsymbol{\xi}) = \begin{cases} 1 & \text{if } |\boldsymbol{\xi}| < 2f_{\max}/c_0 \\ 0 & \text{otherwise} \end{cases}$$

$$C_2(\boldsymbol{\xi}) = \begin{cases} 1 & \text{if } |\boldsymbol{\xi}| < 2f_{\min}/c_0 \\ 0 & \text{otherwise.} \end{cases}$$

In this case we find that the PSF, $L(\boldsymbol{z},0)$, is a difference of sombrero functions, that is

$$L(z,0) = \frac{4\pi}{|\boldsymbol{z}|c_0}\left(f_{\max}J_1\left(\frac{2|\boldsymbol{z}|f_{\max}}{c_0}\right) - f_{\min}J_1\left(\frac{2|\boldsymbol{z}|f_{\min}}{c_0}\right)\right), \tag{13}$$

where J_n is a Bessel function of the first kind. A cross section of this function is shown in Figure 4a.

In the bistatic case, where both the transmitter and receiver are traversing the same circular path, a single pass results in a data collection manifold that is an annulus of the same width as in the monostatic case. However, the outermost portion of the annulus for the bistatic case will be within the outermost portion of the annulus for the monostatic case. For example for a flight trajectory $\Gamma_T(s) = (R\cos s, R\sin s, h)$, $\Gamma_R(s) = (R\cos s + \vartheta, R\sin s + \vartheta, h)$ the annulus will only contain points such that $|\boldsymbol{\xi}| < \sqrt{2}f_{\max}/c_0$ when $\vartheta = 90$. We call the angle ϑ the bistatic angle. This suggests that for a single pass, image resolution formed from a bistatic setup will be no better than for a monostatic setup. However, by taking multiple passes it is theoretically possible to fill in the empty space in the data collection manifold. This is illustrated in Figure 3, where the outermost annulus represents the data collected for a monostatic CSAR, while the inner annulus represents the data collected for a bistatic setup with a bistatic angle $\vartheta = 30°$. Taking more measurements with larger bistatic angles will "fill in" the empty spaces of the data collection manifold.

Such a data collection manifold results in a point spread function given by (13) when $f_{\min} = 0$. This is shown in Figure 4b. Note that compared to Figure 4a, the side lobes for this best possible case are much less prominent. If we define resolution to be the width of the main lobe, then given that the first zero of the Bessel function $J_1(x)$ occurs when $x \approx 4$, we find that the maximum resolution is

$$R \approx 2c_0/f = 2\lambda \tag{14}$$

where λ is the wavelength.

Here we note our assumption that the target reflects equally from all perspectives. In practice the Radar Cross Section (RCS) of a target is dependent on the incident angle of the radar beam, that is the reflectivity function is dependent on the orientation of the target with respect to the transmitter.[11] Furthermore, the reflected angle, the angle at which the reflected signal leaves the target, is affected by the incident angle. These effects combine such that the reflected signal from the different components of a target are visible only for particular bistatic angles.[12] Thus, it is unlikely for any reconstructed image to approach the maximum resolution.

5. CONCLUSION

In this paper we've analyzed imaging resolution by examining an backprojection operator inversion formula. In particular we've shown that this reproduces previous results for monostatic stripmap SAR. We've also shown how this analysis can lead to better imaging resolution.

REFERENCES

[1] Nolan, C. J. and Cheney, M., "Synthetic aperture inversion," *Inverse Problems* **18**(1), 221–235 (2002).

[2] Nolan, C. and Cheney, M., "Synthetic aperture inversion for arbitrary flight paths and non-flat topography," *Image Processing, IEEE Transactions on* **12**(9), 1035–1043 (2003).

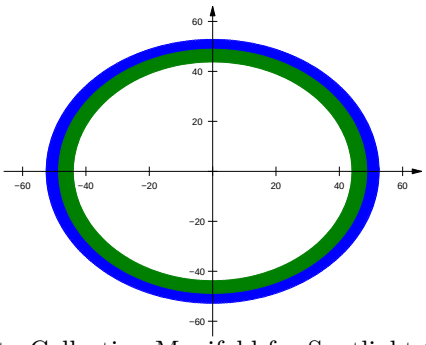

Figure 3: Data Collection Manifold for Spotlight Circular SAR

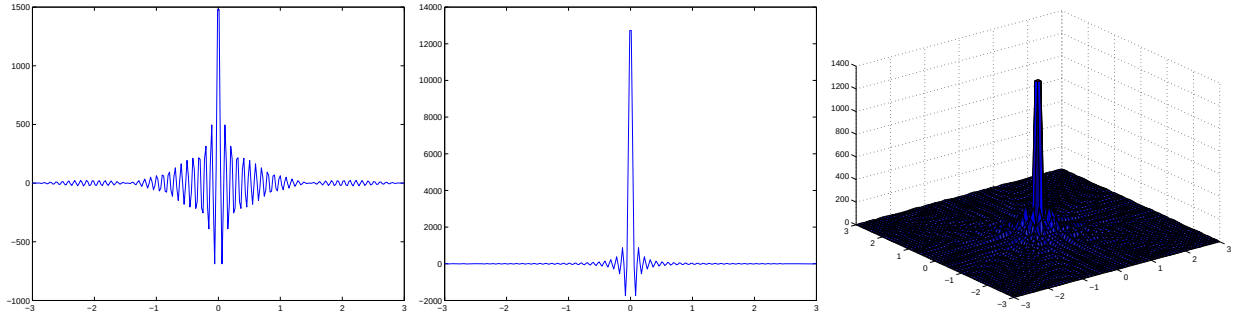

(a) PSF for Single-pass Circular SAR (b) Best PSF Possible (c) 3D View of Best Possible PSF

Figure 4: Point Spread Function of Spotlight Circular SAR

[3] Yarman, C., Yazici, B., and Cheney, M., "Bistatic synthetic aperture radar imaging for arbitrary flight trajectories," *Image Processing, IEEE Transactions on* **17**, 84 –93 (Jan. 2008).

[4] Curlander, J. and McDonough, R., [*Synthetic aperture radar- Systems and signal processing*] (1991).

[5] Carrara, W., Goodman, R., and Majewski, R., [*Spotlight synthetic aperture radar- Signal processing algorithms*] (1995).

[6] Deming, R. W., "Tutorial on fourier space coverage for scattering experiments, with application to sar," in [*Proceedings of SPIE, Algorithms for Synthetic Aperture Radar Imagery XVII*], Zelnio, E. G. and Garber, F., eds., **7699**, SPIE, April (2010).

[7] Yazici, B., Cheney, M., and Yarman, C., "Synthetic-aperture inversion in the presence of noise and clutter," *Inverse Problems* **22**, 1705–1729 (2006).

[8] Hormander, L., [*The analysis of linear partial differential operators IV*], Springer, New York (2009).

[9] Duistermaat, J. J., [*Fourier integral operators*], vol. 130 of *Progress in mathematics*, Birkhäuser, Boston (1995).

[10] Nolan, C. and Cheney, M., "Microlocal analysis of synthetic aperture radar imaging," *Journal of Fourier Analysis and Applications* **10**(2), 133–148 (2004).

[11] Cravey, R., Cha, C., and Burt, E., "Bistatic radar cross section modeling," in [*Antennas and Propagation Society International Symposium, 1988. AP-S. Digest*], 412–415, IEEE (1988).

[12] Glaser, J., "Some results in the bistatic radar cross section (RCS) of complex objects," *Proceedings of the IEEE* **77**(5), 639–648 (1989).